Journal of Controlled Release 362 (2023) 342–355

Contents lists available at ScienceDirect

Journal of Controlled Release

journal homepage: www.elsevier.com/locate/jconrel

Intravitreal implants manufactured by supercritical foaming for treating retinal diseases

Carlos Bendicho-Lavilla [a,b,1], Iria Seoane-Viaño [a,b,c,1], Víctor Santos-Rosales [d], Victoria Díaz-Tomé [a,e], María Carracedo-Pérez [d], Asteria M. Luzardo-Álvarez [a,b], Carlos A. García-González [d], Francisco J. Otero-Espinar [a,b,*]

[a] Department of Pharmacology, Pharmacy and Pharmaceutical Technology, Faculty of Pharmacy, and Materials Institute iMATUS, University of Santiago de Compostela (USC), 15782 Santiago de Compostela, Spain
[b] Paraquasil Group (GI-2109), Health Research Institute of Santiago de Compostela (IDIS), 15706 Santiago de Compostela, Spain
[c] Department of Pharmaceutics, UCL School of Pharmacy, University College London, 29-39 Brunswick Square, London WC1N 1AX, UK
[d] Departamento de Farmacología, Farmacia y Tecnología Farmacéutica, I+D Farma (GI-1645), Facultad de Farmacia, Materials Institute iMATUS and Health Research Institute of Santiago de Compostela (IDIS), Universidade de Santiago de Compostela, 15782 Santiago de Compostela, Spain
[e] Clinical Pharmacology Group, Health Research Institute of Santiago de Compostela (IDIS), 15706 Santiago de Compostela, Spain

ARTICLE INFO

Keywords:
Supercritical foaming utilizing CO_2
PLGA intravitreal implants
Dexamethasone
Monoclonal antibodies
Age-related macular degeneration (ADM)
Three (3D)-dimensional printing

ABSTRACT

Chronic retinal diseases, such as age-related macular degeneration (AMD), are a major cause of global visual impairment. However, current treatment methods involving repetitive intravitreal injections pose financial and health burdens for patients. The development of controlled drug release systems, particularly for biological drugs, is still an unmet need in prolonging drug release within the vitreous chamber. To address this, green supercritical carbon dioxide ($scCO_2$) foaming technology was employed to manufacture porous poly(lactic-*co*-glycolic acid) (PLGA)-based intravitreal implants loaded with dexamethasone. The desired implant dimensions were achieved through 3D printing of customised moulds. By varying the depressurisation rates during the foaming process, implants with different porosities and dexamethasone release rates were successfully obtained. These implants demonstrated controlled drug release for up to four months, surpassing the performance of previously developed implants. In view of the positive results obtained, a pilot study was conducted using the monoclonal antibody bevacizumab to explore the feasibility of this technology for preparing intraocular implants loaded with biologic drug molecules. Overall, this study presents a greener and more sustainable alternative to conventional implant manufacturing techniques, particularly suited for drugs that are susceptible to degradation under harsh conditions.

1. Introduction

Chronic retinal diseases, including age-related macular degeneration (AMD), diabetic retinopathy (DR), or diabetic macular edema (DME), are a leading cause of ocular morbidity and global visual impairment. Notably, AMD stands as the primary cause of blindness in developed countries, particularly among the elderly, and its prevalence is expected to increase due to the exponential aging of the population [1,2]. In the realm of AMD treatment, intravitreal anti-vascular endothelial growth factor (anti-VEGF) therapy stands as the current gold-standard approach. Among the first-line anti-VEGF drugs are bevacizumab, aflibercept, and ranibizumab, which are administered *via* intravitreal injections every 1 to 3 months, depending on the patient's clinical response [3]. In cases where anti-VEGF drugs fail as effective therapy or are not well-tolerated, intravitreal corticosteroids like dexamethasone or fluocinolone have emerged as viable secondary treatment options [4]. The cost associated with providing care for AMD is considerably high due to the treatment burden that entails frequent visits to ophthalmology departments and the expenses related to anti-VEGF drugs [5]. Furthermore, patients who adhere to a regular treatment regimen tend

* Corresponding author at: Department of Pharmacology, Pharmacy and Pharmaceutical Technology, Faculty of Pharmacy and Materials Institute iMATUS, University of Santiago de Compostela (USC), 15782 Santiago de Compostela, Spain.
E-mail address: francisco.otero@usc.es (F.J. Otero-Espinar).
[1] Both authors contributed equally to this work.

https://doi.org/10.1016/j.jconrel.2023.08.047
Received 2 May 2023; Received in revised form 18 August 2023; Accepted 23 August 2023
Available online 4 September 2023

to achieve better visual outcomes compared to those who follow an irregular schedule [6]. Therefore, future treatments for chronic retinal diseases should strive to enhance the longevity of drugs within the vitreous chamber, thus reducing the frequency of injections [7]. Significant progress has been made in this regard since the approval of Ozurdex® (Allergan) in 2014 [8] for the treatment of DME. Ozurdex® is an intravitreal implant composed of a poly(lactic-*co*-glycolic acid) (PLGA) matrix containing 700 μg of dexamethasone, capable of releasing the drug over several months [9]. The implant is placed into the vitreous cavity of the eye through a small incision in the sclera, which is created by an ophthalmologist using a specialised instrument, after applying local anaesthesia.

Recent research has been dedicated to the development of long-acting drug delivery systems that offer extended release of drugs within the vitreous chamber [5,10]. However, current manufacturing techniques for implantable devices often involve harsh fabrication conditions, such as high temperatures or the utilisation of organic solvents [11–16]. One prevalent technique, material extrusion, necessitates elevated temperatures that can lead to structural damage and a decrease in therapeutic efficacy for heat-sensitive drugs, including biologics. To address these limitations, alternative approaches such as solvent casting have been explored, which employ organic solvents as substitutes for high temperatures. Nevertheless, organic solvents are generally recognised as non-thermodynamically stable and toxic substances that pose risks to both human health and the environment. Consequently, endeavours in the field are focused on the development of greener technologies that are both safe for organisms and employ mild processing conditions [17–20].

Supercritical fluid technology, utilising supercritical CO_2 ($scCO_2$), has emerged as a versatile processing platform for manufacturing highly customisable, drug-loaded structures without the need for organic solvents or high temperatures [21–23]. The mild conditions at the critical point of CO_2 (7.38 MPa and 304 K) enable the processing of polymeric structures that efficiently incorporate thermolabile drug molecules, particularly biologics, with high yields [24,25]. One key application of this technology is supercritical foaming, which involves using $scCO_2$ as a porogen to produce polymeric implantable devices loaded with drugs and with adjustable shapes and textural characteristics, including pore size distribution and interconnectivity. The process of supercritical foaming occurs in two stages. In the first stage, CO_2 is absorbed and dissolved into the polymeric matrix under high pressure, resulting in polymer swelling. In the second stage, the system is depressurised, leading to the formation of a porous structure with controlled porosity [24,25]. The porous structure of the medicated implant plays a crucial role in regulating the drug release profile and can be optimised by adjusting various operating parameters, such as temperature, pressure, contact time, and depressurisation rate [26–30]. These parameters can be fine-tuned to achieve desired release kinetics and enhance therapeutic efficacy.

Given the current need to develop long-acting intravitreal drug delivery systems and alleviate the treatment burden associated with existing therapies, this study aims to investigate the viability of producing PLGA-based intravitreal implants using supercritical foaming. Customised moulds with specific geometries were created through stereolithography (SLA) 3D printing to facilitate the manufacturing process [31]. The use of 3D printing to produce the moulds is primarily advantageous due to its simplicity and cost-effectiveness, which is particularly beneficial in a research setting. Moulds can be adjusted in terms of size, shape, and composition, and their reusability further contributes to their practicality. Dexamethasone, a commonly used corticosteroid for treating chronic retinal diseases, was chosen as the model drug. The selection of PLGA as the matrix material was based on its biodegradability, biocompatibility, and favorable foaming properties. The study primarily focused on assessing the impact of slight modifications in depressurisation rates [32,33] on the morphological properties of the foamed implants and their subsequent *in vitro* drug release. In addition, comprehensive characterisation of the implants was performed to evaluate their physicochemical properties, biocompatibility, and cytotoxicity. In the light of the results obtained from the initial batch of implants, further experiments were performed to explore the potential of incorporating biologic drugs into the implants. To achieve this, a proof-of-concept study involving the monoclonal antibody bevacizumab was conducted. Bevacizumab was chosen as the model drug due to its susceptibility to degradation under harsh processing conditions such as high temperatures and pH changes [34].

2. Materials and methods

2.1. Materials

Resomer® RG 503H (RES) (Mw: 10 kDa; lactide:glycolide = 50:50) was purchased from Evonik (Essen, Germany), Purasorb® PDLG 5002A (PUR) (Mw 16 kDa; lactide:glycolide = 50:50) was purchased from Purac (Gorinchem, The Netherlands), dexamethasone (DEX) base was purchased from Acofarma (Barcelona, Spain), bevacizumab (BEV) (Avastin®) was purchased from Roche (Basel, Switzerland). Hydroxypropyl-β-cyclodextrin (HPβCD) was purchased from Roquette (Lestrem, France). The clear 3D printing resin (Anycubic resin UV wavelength 405 nm) was obtained from Shenzhen Anycubic Technology Co. Ltd., (Shenzhen, China). Culture media, FBS and all supplements were purchased from Biological Industries (Cromwell, CT, USA).

2.2. Methods

2.2.1. Manufacturing of 3D printed moulds

Moulds were designed using Autodesk Fusion 360 (Autodesk, CA, US). The design consisted of two halves, with a funnel shape in the upper part and a tubular shape in the lower part (Fig. 1). Both halves were securely attached using a pressure screw system, which prevented powder leakage during processing. The CAD file was exported in .stl format and processed in the Photon Workshop (Shenzhen, China) slicer software. The slice parameters were set to 0.05 mm layer thickness, 5 s normal exposure time, 0.05 s off time, 30 s bottom exposure time, and 4 bottom layers. The sliced mould file was then loaded into the SLA 3D printer (Anycubic Photon Mono X 6 K, Shenzhen Anycubic Technology Co., Ltd., Shenzhen, China). The 3D printer was filled with clear 3D printing resin and a batch of 20 moulds was printed. The 3D printed moulds were then washed with isopropanol in an ultrasonic bath and cured in a UV light cabinet for 1 min on each side.

2.2.2. Manufacture of implants by supercritical foaming

A preliminary study was conducted to select the optimal blend of PLGAs for the foaming process. Several blends were tested, including RES:PUR (50:50), RES:PUR (25:75), RES:PUR (75:25), and RES:PUR (40:60) and (60:40). Additionally, moulds with varying sizes of the tubular part (5, 10, 15, and 20 mm) were tested to assess their impact on the foaming process. The effect of covering the inlet funnel with Parafilm® M sealing film, silicone, or leaving it uncovered was also evaluated. The components of the implants, in the form of dry powders, were weighed according to the proportions specified in Table 1, physically mixed in a mortar, and ground with a pestle. The dose of each drug was selected to match the doses administered in clinical practice.

For BEV implants, a previous purification step of the commercial formulation of bevacizumab (Avastin®) was necessary. Avastin® was purified using an Amicon® Ultra-2 mL centrifuge filter (NMWL 30 kDa) (Millipore®, Burlington, Massachusetts, USA) to remove the excipients included in the commercial formulation. The purified BEV solution was then resuspended in Milli-Q® water and 8% (*w*/w) hydroxypropyl-β-cyclodextrin (HPβCD) was added to the solution to act as an anti-aggregant and cryoprotectant [35–37]. HPβCD was found not to be toxic or irritating for ocular use [38]. The resulting solution was then freeze-dried to obtain the monoclonal antibody in powder form. The solutions

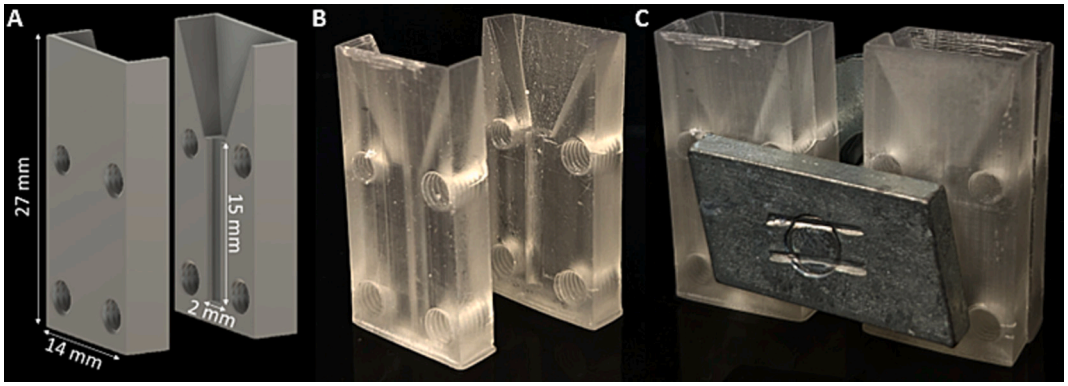

Fig. 1. (A) CAD design of the intravitreal implant mould with the desired dimensions. (B) Gross view of a 3D-printed mould with a funnel shape to facilitate powder loading. (C) View of the moulds assembled with a pressure screw system.

Table 1
Implant composition % (*w*/w) and depressurisation rates (g/min) of implants containing PLGA, DEX, BEV and HPβCD processed by supercritical CO_2 foaming.

Implant	Depressurisation (g/min)	RES %(w/w)	PUR %(w/w)	DEX %(w/w)	BEV %(w/w)	HPβCD %(w/w)
1.8DEX	1.8	46.7	46.7	6.6	–	–
3.6DEX	3.6	46.7	46.7	6.6	–	–
7.2DEX	7.2	46.7	46.7	6.6	–	–
3.6BEV	3.6	41	41	–	10	8

were frozen at −80°C and then freeze-dried using a LyoQuest freeze-dryer (Telstar, Terrassa, Barcelona) with a final condenser temperature of −53°C.

A second-derivative ultraviolet spectrum was carried out using a UV–Vis spectrophotometer (Agilent Cary 60 UV–Vis, Santa Clara, California, USA) to verify the integrity of the BEV structure in Avastin® solution, freeze-dried Avastin® and purified and freeze-dried Avastin® with 8% (*w*/w) HPβCD before and after the processing with supercritical CO_2 [39].

The powder blends were loaded into the 3D-printed moulds and compacted with a compression rod. The moulds were then placed in a 100 mL-high-pressure stainless steel autoclave (Thar Technologies, Pittsburgh, PA, USA). The supercritical foaming was carried out following a pressurisation-soaking-single depressurisation stepwise protocol. CO_2 was pressurized into the autoclave at 5 g/min until a pressure of 100 bar was reached, and the temperature was maintained at 35°C. The system was left under stirring at 700 rpm in batch mode for 1 h (soaking period). Subsequently, the autoclave was depressurised at a venting rate of 1.8, 3.6 or 7.2 g/min for DEX implants and at 3.6 g/min for BEV implants until atmospheric pressure was reached. The implants were stored overnight at 4°C to allow complete CO_2 desorption.

2.2.3. Structure analysis

The dimensions of the implants, including diameter and length, were measured with a digital Vernier calliper. The mass of each implant was determined using an analytical balance (Sartorius Quintix 35-1S). The morphological analysis of the implants was conducted by observing the external structure of the implants through a stereomicroscope with an electronic camera (Olympus® SZ-CTV/Olympus® SC100). The surface topography and internal structure of the implants were examined using field emission scanning electron microscopy (FESEM) (ZEISS EVO LS15). The sample surface was imaged at 20 kV using the backscattered electron detector (BSD) under variable pressure (VP) conditions. The implants and their transversal cuts were fixed on 25 mm aluminium stubs using self-adhesive carbon discs prior to the analysis.

The microstructure of the implants was analysed by microcomputed tomography (Micro-CT) using a Skyscan 1272 high resolution X-ray 3D micro-CT equipped with an 11 MP X-ray detector (Bruker, Kontich, Belgium). The implants were imaged at 2 μm pixel resolution, 50 kV and 200 μA without filter. Projections were collected with a rotation step of 0.5° for 180° with an exposure time of 900 ms, and then reconstructed and analysed using NRecon and CTvox software (Bruker, Kontich, Belgium), respectively. For 3D analysis, slices were converted into binary images using a threshold of 70–255 and a volume of interest (VOI) of 53 mm^3 was chosen to evaluate total porosity, pore size and interconnectivity.

2.2.4. Texture analysis

Texture analysis was performed using a precision Universal Testing Machine AGX-X series (Shimadzu, Kyoto, Japan), equipped with a 50 N load cell and Trapezium X software (Shimadzu, Kyoto, Japan). For this purpose, a blade was secured in the upper support, while the implant was positioned on the lower plate. The blade was then gradually lowered at a speed of 1 mm/min until the implant ruptured. The force-displacement curve was subsequently recorded, from which three key material parameters were derived: rupture strength, failure work, and elasticity.

Breaking strength was determined as the maximum force observed at the point of material fracture, corresponding to the highest force recorded on the force-displacement curve. Failure work was calculated as the area under the curve (AUC) between force and displacement until the breaking strength was reached. Elasticity was assessed using the modulus of elasticity, known as Young's modulus, which is the ratio between force and deformation obtained from the slope of the force-displacement curve.

2.2.5. Drug distribution in the implant

The distribution of DEX within the implants was analysed using energy dispersive X-ray analysis (EDX) and Raman spectroscopy. For EDX, a semi-quantitative microanalysis and distribution mapping of the elemental composition of the surface and the core of the DEX implants was conducted using an EDS Ultim® Max (Oxford Instruments, Abingdon, United Kingdom) controlled by INCA software (Oxford Instruments, Abingdon, United Kingdom). The acquisition conditions were 20Kv and a working distance of 8.5 mm for a more precise analysis. The same analysis was performed on the DEX implants after the *in vitro* release assay.

Raman spectra were recorded at room temperature on a Raman confocal microscope alpha300 R (WITec, Ulm, Germany) using a 532 nm laser with a power of 7 mW. The implants were sliced and placed in a sampler holder to examine the core of the implant. A total area of 70 × 70 μm was recorded with a lateral resolution of 1 spectrum every 300 μm, for a total of 19,600 spectra. Project Five 5.3 (WITec, Ulm, Germany) was used for data processing and imaging.

2.2.6. Crystallinity

The crystal structure and thermal stability of DEX, PLGA powders, implants, and the physical mixture of PLGA and DEX were identified and characterised using X-ray powder diffraction (XRD) and differential scanning calorimetry (DSC). XRD measurements of the powdered samples were measured with Bragg-Brentano geometry using a Bruker D8 Advance diffractometer (Bruker, Massachusetts, USA) (40 kV, 40 mA, theta/theta) equipped with a Cu sealed X-ray tube (CuKα1 ($\lambda = 1.5406$ Å) and a LYNXEYE XE-T detector). The diffractograms were obtained in the 2θ angle range 3°–40°with a step of 0.02° and a counting time of 2 s per step. The thermal properties of DEX, PLGA powders, implants, and the physical mixture of PLGA and DEX were determined using a TA Instruments® Q1000 DSC/TGA/IR analyser (TA Instruments, Newcastle, USA). Samples were heated from 0°C to 400°C at a rate of 5°C/min under nitrogen atmosphere.

2.2.7. Drug content

To measure the drug loading of the DEX implants, 3 mg of each implant were dissolved in 5 mL of acetonitrile ($n = 3$). Subsequently, DEX concentrations were measured using a Cary 60 UV–Vis spectrophotometer (Agilent, Santa Clara, California, USA) at a UV wavelength of 241 nm.

2.2.8. In vitro drug release

DEX and BEV release patterns were recorded by placing loaded implants (3 replicates of each processing condition) in glass vials with 3 mL of phosphate-buffered saline (PBS) at physiological pH (7.4). Vials were kept in an orbital shaker at 37°C under constant orbital movement (100 rpm). At predetermined times, 0.5 mL aliquots were withdrawn from the medium and replaced with the same volume of fresh medium. DEX concentrations were measured using the method described above (2.2.7. Drug content) and the pH of the samples was measured with a Hanna® HI5522 pH meter (Hanna Instruments, Eibar, Spain) at each time point.

Samples of BEV solutions were filtered through 0.22 μm PVDF filters (Millipore®, Burlington, Massachusetts, USA) and the concentration of the drug was determined with high-performance liquid chromatography (ACQUITY UPLC H-Class Plus, Waters, Milford, Massachusetts, USA) with an FTN injector and PDA detector. The stationary phase was a BioResolve RP mAb Polyphenyl, 450 Å column, 2.7 μm, 2.1 × 50 mm (Waters, Massachusetts, USA), and the mobile phase was a gradient from 15% water 0.1% trifluoroacetic acid (TFA) and 85% acetonitrile 0.1% TFA to 85% water 0.1% TFA and 15% acetonitrile 0.1% TFA. The flow rate was set to 0.8 mL/min, with an injection volume of 1 μL, a column temperature of 80°C, and a UV wavelength of 280 nm. The elution time of BEV was approximately 2.4 min. Data were processed using Empower 3 software (Waters, Milford, Massachusetts, USA).

2.2.9. Biocompatibility assessment of the implants

2.2.9.1. Hen's egg test on the chorioallantoic membrane (HET-CAM). The HET-CAM test was used to assess whether the implants would cause ocular irritation, following the method previously described by the Interagency Coordinating Committee on the Validation of Alternative Methods (ICCVAM) [40]. Fertile Broiler chicken eggs were placed in an incubator YZ-56S for 9 days at 38 ± 0.5°C and 65% relative humidity. On day 9, the eggshell was carefully removed from the widest end of the egg to expose the CAM. Afterwards, 300 μL of drug release medium ($n = 3$) from day 135 and 5 of the DEX and BEV implants, respectively, were applied to the CAM. Three possible reactions, if applicable, were monitored for 5 min: haemorrhage, vascular lysis, or coagulation of the vessels. 0.9% NaCl and 0.1 N NaOH solutions were used as negative and positive controls, respectively.

2.2.9.2. Cytocompatibility studies with the ARPE-19 cell line. The ARPE-19 cell line was used due to its morphological and functional characteristics similar to adult retinal pigment epithelium (RPE) cells. ARPE-19 cells (ATCC®, American Type Culture Collection, Manassas, VA, USA) were cultured in F-12/DMEM medium supplemented with 10% inactivated Foetal Bovine Serum (FBS), 2 mM L-alanyl-L-glutamine and 1% of an antibiotic/antimycotic mixture (10,000 units/mL penicillin G, 10 mg/mL streptomycin and 10 mg/mL neomycin). Cell culture was maintained at 37°C, under a 5% CO_2 atmosphere with 95% relative humidity, in 25 and 75 cm^2 T-Flasks. For maintenance, sub-confluent cultures (80%) were split using 0.25% trypsin/EDTA.

To determine the viability of ARPE-19 cells in the formulations, an assay based on the metabolization of a tetrazolium salt (XTT) was used. The tetrazolium salt is metabolised by viable cells leading to a water-soluble formazan salt that is quantifiable spectrophotometrically at 450 nm [41]. XTT sodium salt (1 mg/mL) in phenol-red free F12/DMEM and phenazine methosulfate (PMS) in PBS (3 mg/mL) solutions were prepared and stored at −80°C. Immediately before performing the assay, XTT and PMS solutions were mixed at a ratio of 1:400 to obtain the activated XTT reagent.

ARPE-19 cells (10,000 cells/well) were seeded in 96-well plates and maintained at 37°C with 5% CO_2. The BEV and DEX implants were sterilised under UV light and incubated in F12/DMEM low serum cell culture medium (37°C; 100 rpm). Samples from BEV implants were taken on days 1 and 7 while samples from DEX implants were taken on days 1, 7, 14 and 21. At one-week intervals, ARPE-19 cells were co-incubated with 100 μL extracts obtained from the implants. After incubation, 50 μL of activated XTT reagent was added to each well and the plate was incubated at 37°C protected from light for 4 h. The absorbance at 450 nm was determined and the number of viable cells was calculated according to a calibration curve in the range of 15,000–234 cells per well. The results were expressed in terms of cell viability percentage with respect to the negative control, which corresponds to ARPE-19 cells cultured in regular growth medium without any treatment. The experiments were performed in triplicate.

3. Results and discussion

3.1. Manufacturing of dexamethasone-loaded implants

In this work, a novel approach for manufacturing intravitreal implants using supercritical foaming was investigated. Customised implants with specific dimensions (10 mm × 2 mm) were prepared by designing 3D printing moulds with precise geometries using an SLA 3D printer, aiming for future clinical applications. The high-resolution capability of the 3D printing technique enabled the production of moulds with accurate geometries [31]. The selected 3D printing resins were acrylic polymer-based [42], and preliminary findings indicated their suitable permeability to supercritical CO_2, making them appropriate for use in the supercritical foaming process to obtain porous structures. The moulds were composed of two parts, which when assembled, created a funnel and a tube. The function of the funnel was to facilitate the dosing of the powder, ensuring homogeneous batches with precise drug doses, which is particularly relevant for expensive drugs such as monoclonal antibodies and other biopharmaceuticals. The tube securely held the powder in place, shaping the implant during the supercritical CO_2 processing.

The two types of PLGA utilised in this study were chosen based on their molecular weight, as it is a crucial factor in determining degradation kinetics. Low molecular weight PLGAs with low inherent viscosity were selected to achieve a release duration of <3 months [43,44]. On the other hand, higher molecular weight polymers possess longer polymeric chains and consequently higher intrinsic viscosity. This results in a slower degradation rate, which is not desirable for the objectives of this study since complete polymer degradation was intended to coincide with the completion of drug release. Furthermore, the 50:50 lactic/glycolic acid ratio and the presence of free carboxylic acid groups enhance the hydrophilicity of the polymer [45].

Supercritical CO_2 foaming parameters were set at moderate pressures (100 bar), mild temperatures (35°C), and short soaking times (1 h). These processing conditions were chosen because they are suitable for thermolabile compounds, such as monoclonal antibodies, as they aim to achieve adequate polymer foaming while maintaining the drug's activity. When using PLGA blends with a RES:PUR ratio exceeding 50:50, uncontrolled foam expansion was observed, while below this threshold, the polymer blend exhibited low expansion rates (data not shown).

Therefore, the optimal blend for further foaming testing was selected as a 50:50 ratio. In terms of mould optimisation, the best results were achieved with uncovered 15 mm moulds. This approach allowed the production of PLGA implants with high porosity, a smooth and non-porous surface, and excellent pore interconnectivity.

3.1.1. Dexamethasone crystalline state in the implants

XRPD and DSC analyses were conducted to examine the physical state of DEX in the implants. Previous literature has described two polymorphic crystalline forms of DEX [46], known as Form A and B, which exhibit similar physical and dissolution properties. The XRPD pattern of pure DEX exhibited prominent peaks at $2\theta = 8.1$, 12.6, 13.7, 14.6, 15.15, 16.25, and 17.85 (Fig. 2), corresponding to the polymorphic crystalline Form A of DEX. The PLGA material displayed a characteristic broad peak at $2\theta = 10–25°$. In the implants containing DEX and PLGA, the distinct peaks of pure DEX powder were observed, indicating the presence of DEX in the crystalline Form A. Conversely, these distinct dexamethasone peaks were not detected in the blank implant sample.

DSC results revealed that DEX exhibited a melting endotherm with an onset temperature of 250°C (Fig. 3). This value was slightly higher than the previously reported onset temperature for the polymorphic crystalline Form A, which was 242°C [46]. The melting endotherm of DEX is complex, involving a melting/recrystallization process between Form A and Form B, resulting in a broader endothermic peak [46]. RES PLGA exhibited two distinct thermal events: a glass transition temperature (Tg) of 49.5°C and a degradation endotherm starting at 300°C. On the other hand, PUR PLGA showed a barely observed Tg event at around 40°C, and the thermal degradation began at higher temperatures compared to RES PLGA. This can be attributed to the lower molecular weight of PUR PLGA (17,000 Da) compared to RES PLGA (24000–38,000 Da). The implants, prepared using a blend of both PLGAs, displayed a thermal event around 50°C, corresponding to the Tg of the polymer.

The melting peak of DEX was not detected in the DEX implants or the physical mixture of DEX and PLGA. However, XRPD analysis indicated the presence of some degree of crystallinity in the DEX implants, similar to that observed in the physical mixture of PLGA and DEX powders. The absence of a drug melting endotherm in the DSC analysis could be attributed to the dissolution of the drug in the melted PLGA, even if drug crystals are present in the implants. One possible explanation for the presence of DEX in a crystalline state within the implant could be the recrystallisation of DEX occurring during storage prior to the assessment of crystallinity [47].

3.1.2. Morphological characterisation of dexamethasone-loaded implants

The implants exhibited satisfactory handling properties and a smooth surface. They also demonstrated good uniformity in their physical dimensions, as indicated in Table 2, and no noticeable macroscopic morphological differences were observed between the formulations, as shown in Fig. 4. The inclusion of DEX led to a slight increase in the weight and length of the implants, which was determined to be statistically significant ($\alpha < 0.05$); however, this increase was considered negligible.

SEM images of the surface and core of the DEX implants are depicted in Fig. 4. The implants exhibited a porous core enveloped by a non-porous outer skin layer measuring 100–140 μm in thickness, which is a typical characteristic of scCO2 foamed materials [48]. The core displayed pore sizes ranging from 20 to 150 μm, and interconnected pores were observed within larger pore cavities. Notably, no drug crystals were detected in the SEM images.

The morphological properties of the DEX-loaded implants were subjected to additional analysis using Micro-CT and 3D reconstruction techniques, as illustrated in Fig. 4. Porosity data obtained from the implants are summarized in Table 3. It was observed that all the implants exhibited a highly porous structure, with overall porosity values exceeding 68%. However, significant differences were observed between different formulations.

The highest pore diameters (77.33 ± 11.38 μm) were achieved in the implants processed at a slower depressurisation rate of 1.8 g/min ($\alpha < 0.05$). Higher depressurisation rates of 3.6 and 7.2 g/min resulted in smaller pore diameters (53.99 ± 2.97 μm and 54.44 ± 5.09 μm, respectively) as shown in Table 3 and Fig. 5A. An increasing trend was observed for the pore throat sizes in implants processed with longer depressurisation rates, as shown in Fig. 5B. The homogeneity of the implants was also affected, with narrower pore size distributions observed in implants processed under higher depressurisation rates [30]. These aspects are illustrated in Fig. 5A and B. The findings of this study align with the principles of classical nucleation theory [49]. Specifically, for a fixed temperature and soaking time, rapid depressurisation promotes nucleation overgrowth (pore formation) and results in a greater number of pores with smaller diameters. Conversely, a decrease in the depressurisation rate leads to larger pores due to increased pore growth and coalescence. This phenomenon also

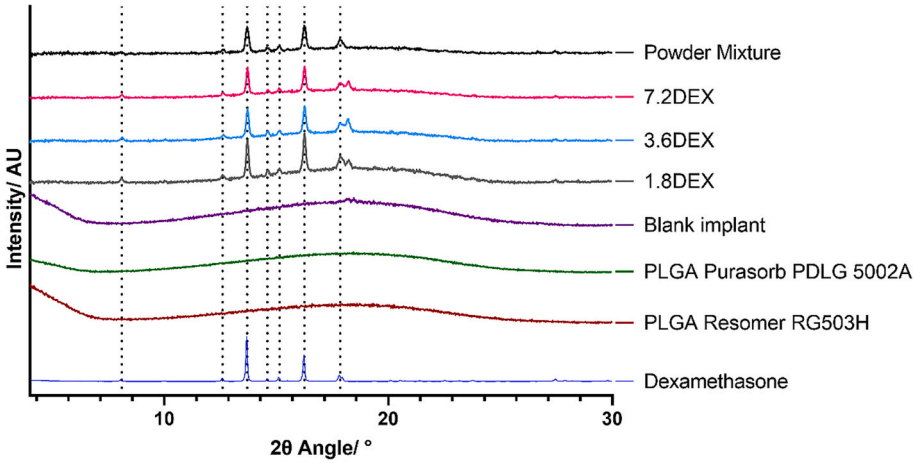

Fig. 2. X-ray powder diffractograms of the drug DEX, PLGA powders, implants, and the physical mixture of PLGA and DEX.

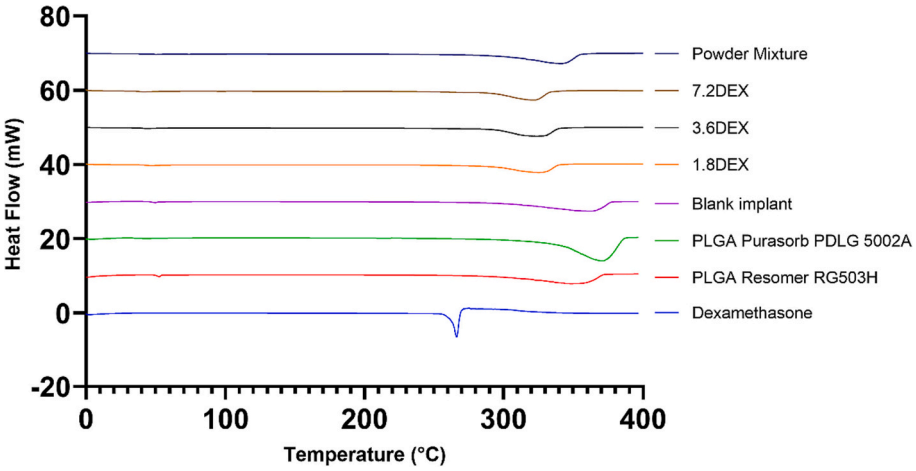

Fig. 3. DSC curves of DEX, PLGA powders, implants, and the physical mixture of PLGA and DEX (Exo Up).

Table 2
Physical properties of dexamethasone implants ($n = 3$).

Implant	Weight ± SD (mg)	Length ± SD (mm)	Diameter ± SD (mm)
Blank	9.97 ± 0.27	8.51 ± 0.07	1.73 ± 0.21
1.8DEX	10.35 ± 0.28	9.54 ± 0.19	1.88 ± 0.01
3.6DEX	10.35 ± 0.18	8.47 ± 0.09	2.02 ± 0.04
7.2DEX	11.14 ± 0.46	9.37 ± 0.35	1.85 ± 0.00

influences the degree of interconnectivity within the structures.

3.1.3. Texture analysis

Fig. 6 shows the key parameters related to the texture analysis of the implants. An evident linear relationship exists between rupture strength, elasticity, and failure work, and the depressurisation rate employed during the process. These variations in the analysed parameters can be attributed to the porous structure of the implants achieved under different conditions. Notably, implants produced at a depressurisation rate of 1.8 g/min, which exhibited larger pore diameters, demonstrated reduced mechanical strength.

The rupture strength values were similar to, or even higher than,

Table 3
Micro-CT porosity data analysis of DEX implants ($n = 3$).

Implant	Pore diameter (μm)	Pore throat (μm)	Open porosity (%)	Overall porosity (%)
1.8DEX	77.33 ± 11.38	31.13 ± 4.01	71.73 ± 2.73	71.74 ± 2.73
3.6DEX	53.99 ± 2.97	25.81 ± 1.01	68.60 ± 2.88	68.61 ± 2.89
7.2DEX	54.44 ± 5.09	24.65 ± 1.16	69.08 ± 1.78	69.09 ± 1.78

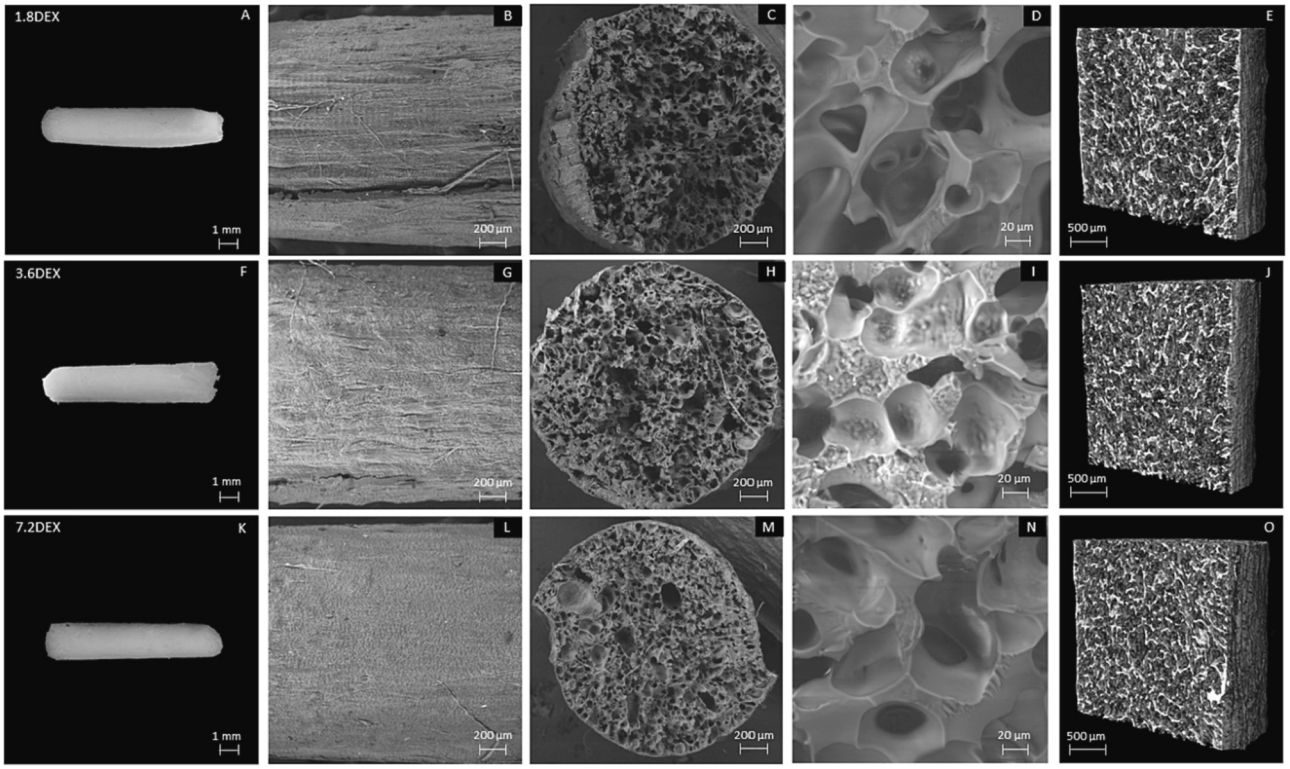

Fig. 4. Stereomicroscopy pictures of the implants (A,F,K). SEM images of the surface and cross-sections of the implants (B,C,D,G,H,I,L,M,N). 3D reconstructions with Micro-CT computed tomography data of the 1.8DEX, 3.6DEX and 7.2DEX implants (E,J,O).

Table 4
Elemental analysis data of the DEX implants core, surface and DEX released implant.

Implant	Distribution	Element (%)		
		Carbon	Oxygen	Fluor
1.8DEX	Core	50.9	47.8	1.2
	Surface	40.0	14.5	45.1
	Released implant surface	32.46	3.13	62.76
3.6DEX	Core	51.4	47.9	0.8
	Surface	35.8	12.8	51.4
	Released implant surface	33.69	11.59	45.73
7.2DEX	Core	50.9	48.3	0.8
	Surface	44.8	19.9	35.0
	Released implant surface	32.2	2.47	64.62

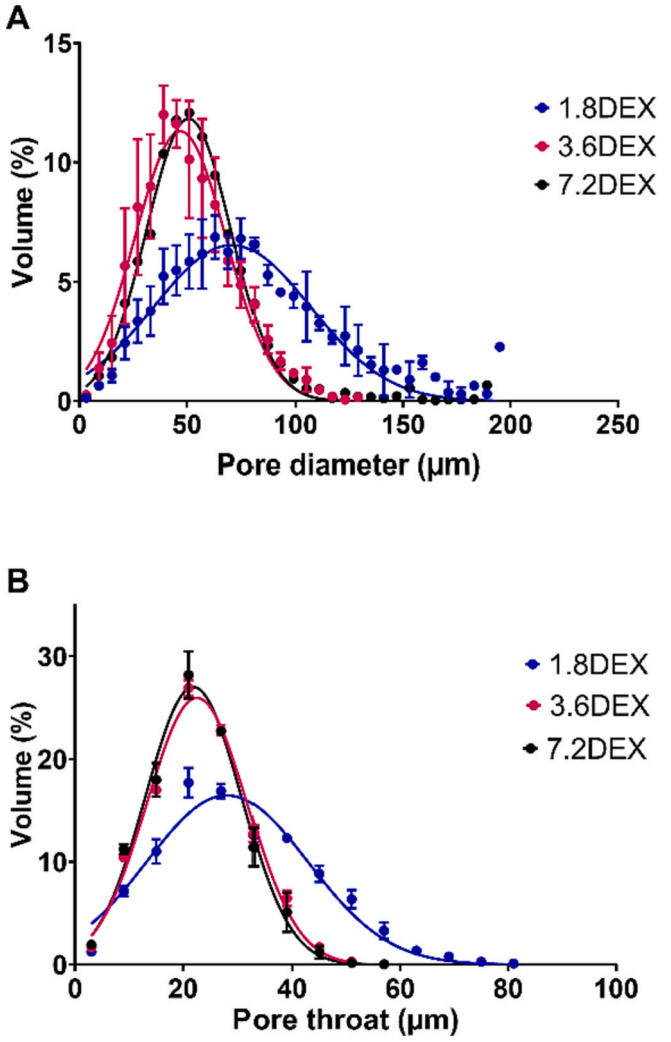

Fig. 5. (A) Pore size and (B) pore throat distributions of the DEX implants calculated through Micro-CT.

those reported in a previous study [50] where intracochlear PLGA implants were produced using hot melt extrusion. The intracochlear implants were compared to Ozurdex® implants in terms of breaking force, resulting in values of 5.33 N for intracochlear implants prepared with 90% PLGA and 10% dexamethasone, and 2.70 N for Ozurdex® implants.

3.1.4. Dexamethasone distribution in the implants

Fig. 7 displays the EDX mapping images of the surface and core of the DEX-loaded implants, as well as the released implants. The distribution of the drug within the implant was determined by the presence of the fluorine atom in the DEX molecule, which is absent in the PLGA molecule. Consequently, a higher concentration of DEX was observed on the surface of the implants, while the core exhibited a lower concentration.

However, Raman confocal microscopy images obtained from longitudinal sections of the implants at higher magnification (Fig. 7) revealed the presence of DEX within the core of the implants processed under all three depressurisation rate conditions. In all cases, aggregates smaller than 10 μm were observed dispersed in the PLGA matrix. These results suggest that DEX is present in higher concentration on the surface than in the core of the DEX-loaded implant. During the depressurisation process, the DEX that is solubilised in the supercritical CO_2 might tend to distribute towards the surface of the implant while the foam is created.

3.1.5. Dexamethasone content and release from the implants

The drug loading of the DEX implants was assessed, yielding values of 98.41 ± 5.05%, 97.76 ± 4.34%, and 98.13 ± 4.17% for 1.8DEX, 3.6DEX, and 7.2DEX, respectively. These findings serve as confirmation of the remarkable drug loading capacity achieved through supercritical foaming.

Fig. 8 illustrates the release profiles of DEX from the implants, demonstrating a controlled release of the drug for a minimum of 60, 75, and 120 days for 1.8DEX, 3.6DEX, and 7.2DEX implants, respectively. To validate the role of the PLGA matrix in regulating drug release, DEX base powder (700 μg) was dissolved in the same volume of medium, and samples were collected and analysed at predetermined time points. Consequently, DEX completely dissolved in the medium within 8 days, highlighting the effective control exerted by the polymeric matrix on drug release. Following this controlled release stage, the release of the drug reached a plateau or even decreased for 1.8DEX and 3.6DEX implants. In the case of 7.2DEX implants, the drug release was extended until the recorded drug concentration levels in the release medium matched those obtained with the DEX solution. On day 135, a one-way ANOVA statistical test was conducted, indicating that the amount of drug released by 7.2DEX was significantly higher ($\alpha < 0.05$) compared to the amount released by 1.8DEX and 3.6DEX, with no statistically significant differences observed between the latter two (α n.s.).

According to Fig. 8, a noticeable decline in the pH levels of the release medium was observed, reaching below pH 3 after day 10. This acidic environment is a result of the hydrolysis of the PLGA, causing the degradation of polymer chains and the production of lactic and glycolic acids. These acids are highly acidic and water-soluble, classified as short-chain fatty acids [51]. Additionally, despite the intended pH maintenance at 7.4 through the use of PBS, the pH drop can be attributed to the infrequent medium fluid volume renewals and the extended intervals between sampling [52].

The pH exerts a notable influence on the stability of DEX in solution, with the drug exhibiting greater stability under acidic pH conditions and decreased stability as the pH increases. In a study, the stability of DEX in pediatric formulations was evaluated and accelerated stability tests were conducted at varying pH levels [53]. At pH 7.85 and 60°C, over 90% of the drug degraded within 42 h. However, when the pH was reduced to 2.13, no degradation of DEX occurred within the same study duration. Moreover, DEX degradation has been observed during *in vitro* release in PBS with a pH of 7.4, as demonstrated in certain studies conducted on intravitreal implants [54,55]. These studies employed liquid chromatography-mass spectrometry (LC-MS/MS) analysis to predict the amount of DEX that underwent degradation during *in vitro* release. However, due to the requirement of LC-MS/MS analysis, this particular model could not be applied to the present study.

Implants produced through supercritical foaming exhibit a non-porous external layer and a porous core. In the initial 30 days of the study, the release of DEX from the implants was controlled by the PLGA matrix forming the non-porous external layer. However, subsequent to this period, the pH profile emerged as the primary factor influencing DEX release. In the case of 1.8DEX implants, the release medium's pH

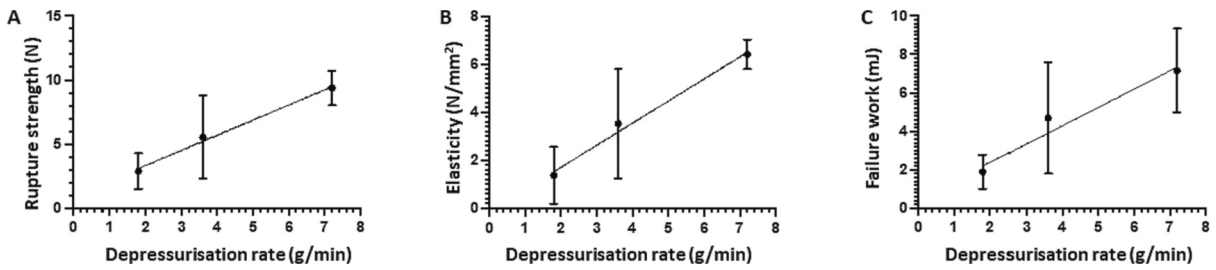

Fig. 6. Texture analysis parameters of the implants, including rupture strength, elasticity, and failure work.

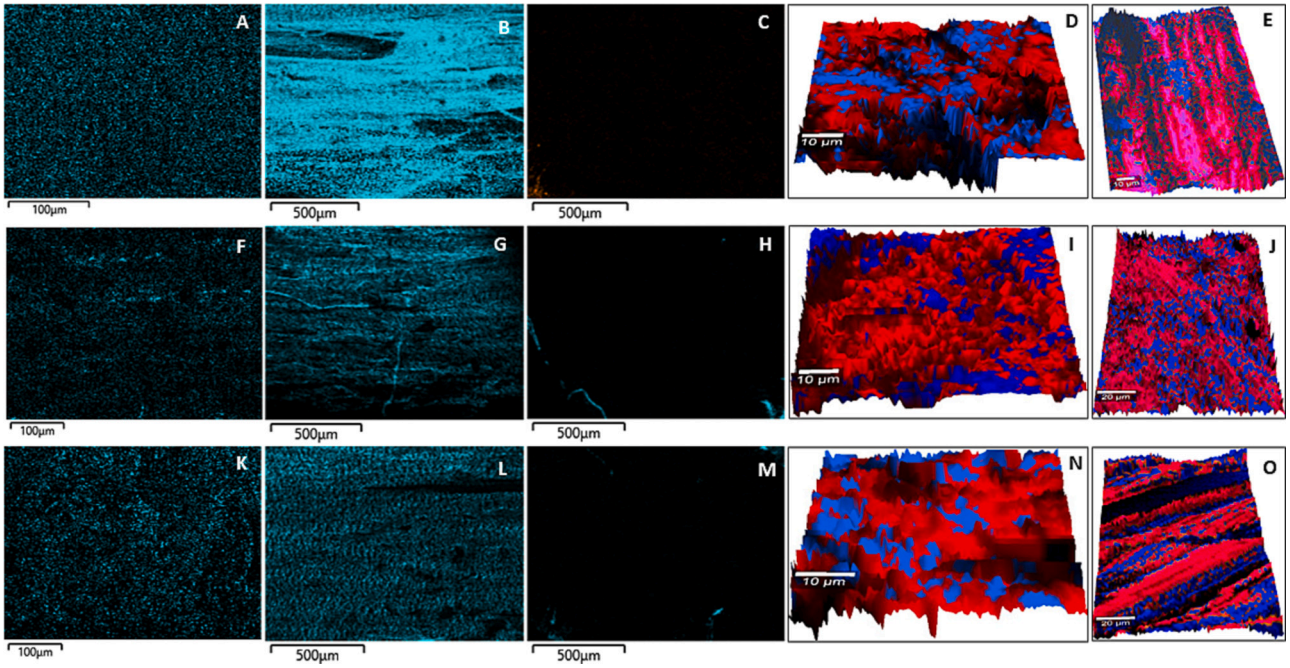

Fig. 7. EDX mapping and Raman confocal microscopy images of the DEX-loaded implants. EDX images reveal the surface of 1.8DEX (A, B), 3.6DEX (F, G), and 7.2DEX (*K*,*L*) implants, as well as the core of 1.8DEX (C), 3.6DEX (H), and 7.2DEX (M) implants. The blue dots indicate the distribution of fluorine atoms. Raman confocal microscopy images depict the distribution of the DEX in the core of 1.8DEX (C, E), 3.6DEX, and 7.2DEX (N, O) implants. Red areas correspond to PLGA and blue areas correspond to DEX. (For interpretation of the references to colour in this figure legend, the reader is referred to the web version of this article.)

Table 4 summarises the element distribution for each implant and location. Furthermore, the presence of fluorine was still observed on the surface of the analysed sample even after the *in vitro* release study, indicating the presence of residual DEX in the implant.

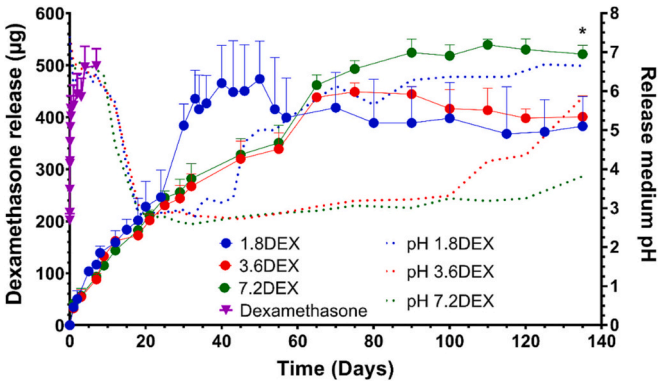

Fig. 8. *In vitro* release profiles of DEX base powder, 1.8DEX, 3.6DEX and 7.2DEX implants and pH changes during DEX release in phosphate buffer pH 7.4 ($n = 3$).

increased more rapidly compared to 3.6DEX and 7.2DEX implants, aligning with the pattern of DEX release from the implant. Subsequently, when the pH of the medium exceeded 5–6, a decline in DEX concentrations was observed due to increased drug degradation. In the case of 3.6DEX implants, the pH elevation took longer, resulting in continued concentration increase up to 75 days, followed by a decline at 90 days, coinciding with the rise in medium pH. Notably, no significant pH increase was observed for the 7.2DEX implants, which released a greater amount of DEX over an extended duration without a decrease in drug concentration. These findings indicate that DEX remains stable under low pH conditions but undergoes degradation at higher pH values.

The transition in release patterns for 3.6DEX and 7.2DEX implants occurred at a later stage compared to 1.8DEX implants. The variations in release behavior and drug degradation rates can be attributed to differences in microstructure, hardness, and the distribution of DEX within the implants. Specifically, among the implants, 1.8DEX exhibited the lowest mechanical strength and the largest pore diameters and throats, facilitating quicker access to the release medium and promoting faster degradation of the polymeric matrix. Additionally, 1.8DEX implants displayed the highest surface concentration of the drug. In contrast, 7.2DEX and 3.6DEX implants showcased smaller pore throats and

diameters, along with higher mechanical strength, and a lower DEX concentration on their surface. This combination contributed to a more favorable drug release pattern.

The results obtained in this study can be compared to previous research that investigated the release of DEX from PLGA implants manufactured using different technologies [56]. For instance, a study examined the *in vitro* release of DEX from intact or fractionated commercial Ozurdex® implants in 30 mL of saline solution [57]. The drug was completely released from the implants within 28 days, and no differences were observed between the fractionated and intact implants. Another study investigated the *in vitro* release of DEX from implants produced through hot-melt extrusion, utilizing 50:50 acid-terminated or ester-terminated PLGAs in 5 mL of PBS [58]. The complete release of the drug was observed after 4–5 weeks (28–35 days). Additionally, the *in vitro* performance of Ozurdex® and DEX cochlear implants, fabricated using hot-melt extrusion with PLGA Expansorb® 50-2A (10,400 Da), was studied in 1 mL of phosphate buffer at pH 7.4 [50]. Ozurdex® exhibited complete drug release within 28 days, and the cochlear implants were able to release 70% of the drug within 10–20 days, reaching 90% after 45 days of testing. In comparison to these examples, the implants developed in this study demonstrated a successful release rate, enabling controlled release of the drug for up to 4 months.

3.2. Manufacturing of bevacizumab-loaded implants

Due to the promising *in vitro* performance of the DEX-loaded implants, a subsequent investigation was undertaken to incorporate thermolabile and complex compounds of interest. In this particular case, the model drug chosen was BEV. To fabricate BEV-loaded implants with an appropriate size-to-drug dose ratio, the dimensions of the moulds were optimised. BEV requires high doses to achieve efficacy (1.25 mg in 0.05 mL of solution). The commercial formulation, Avastin®, contains significant amounts of excipients (trehalose dihydrate, sodium phosphate, and polysorbate 20) to stabilise the monoclonal antibody. Consequently, each implant necessitates large volumes of freeze-dried drug powder. The Avastin® solution underwent purification to eliminate the excipients, and subsequently, it was freeze-dried with 8% (*w*/w) HPβCD, serving as a cryoprotectant and antiaggregant (refer to Methods, Section 2.2), resulting in the obtainment of BEV in powder form.

3.2.1. Bevacizumab stability after freeze-drying

To examine and compare the structural characteristics of monoclonal antibodies, a second derivative ultraviolet absorption spectroscopy analysis was performed. Second derivative spectra enable the differentiation of spectral bands associated with aromatic amino acids, allowing for the detection of changes in the structural state of the monoclonal antibody. The microenvironment of tyrosine residues within the BEV sequence was investigated to compare the BEV structure across all the samples. To accomplish this, the a/b ratio was utilised, where "a" represents the distance between the maximum (~λ287) and minimum (~λ283) absorbance of the negative peak associated with tyrosine, and "b" represents the distance from a second maximum (~λ295) to a minimum (~λ290.5) related to tryptophan [59]. Fig. 9 illustrates the a/b ratios observed in the tested samples. No significant differences were observed in the a/b ratios among all the samples (α n.s.), suggesting comparable protein structures between the resuspension of freeze-dried BEV, the processing with supercritical CO2, and the commercial solution (Avastin®).

3.2.2. Morphological characterisation of bevacizumab-loaded implants

The BEV-loaded implants displayed slightly rough surfaces while maintaining satisfactory handling properties. The results presented in Table 5 demonstrate consistent physical dimensions among the implants, indicating good uniformity. However, the inclusion of lyophilised BEV led to a significant disparity in implant weight ($\alpha < 0.05$), while no notable variations were observed in terms of length or diameter.

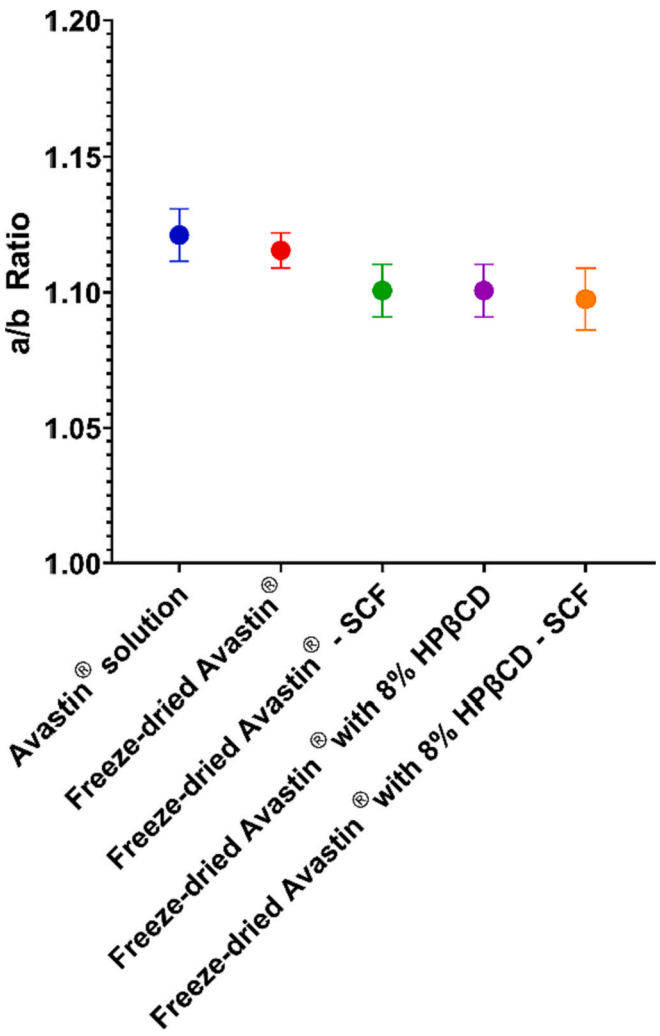

Fig. 9. a/b ratio for Avastin® solution, freeze-dried Avastin® and freeze-dried Avastin® with 8% (*w*/w) HPβCD.

Table 5
Physical properties of BEV implants ($n = 3$).

Implant	Weight ± SD (mg)	Length ± SD (mm)	Diameter ± SD (mm)
Blank	9.97 ± 0.27	8.51 ± 0.07	1.73 ± 0.21
3.6BEV	11.90 ± 0.35	9.73 ± 1.07	1.91 ± 0.10

SEM images of the BEV-loaded implant are shown in Fig. 10. The surface of the implant exhibited an irregular pattern with noticeable macropores, while the inner structure appeared non-porous. In contrast to DEX-loaded implants, the level of porosity within the core of the BEV-loaded implants was lower. Additionally, patches of drug or excipient crystals were observed within the polymeric matrix of the implant core, preventing the formation of a porous structure. This observation could be attributed to the larger volume of drug and excipient powder required for BEV, which impeded the effective foaming of the polymer.

3.2.3. Bevacizumab release from the implants

The release profile of the 3.6BEV implants is shown in Fig. 11, showcasing the results. These implants were loaded with 1.25 mg of BEV powder, which corresponds to the clinically used dosage, and the release kinetics were assessed over a period of 5 days. Notably, the release of BEV was exceptionally rapid, with a release rate of 91.41 ± 10.64% observed on the first day, and complete release was achieved by day 5.

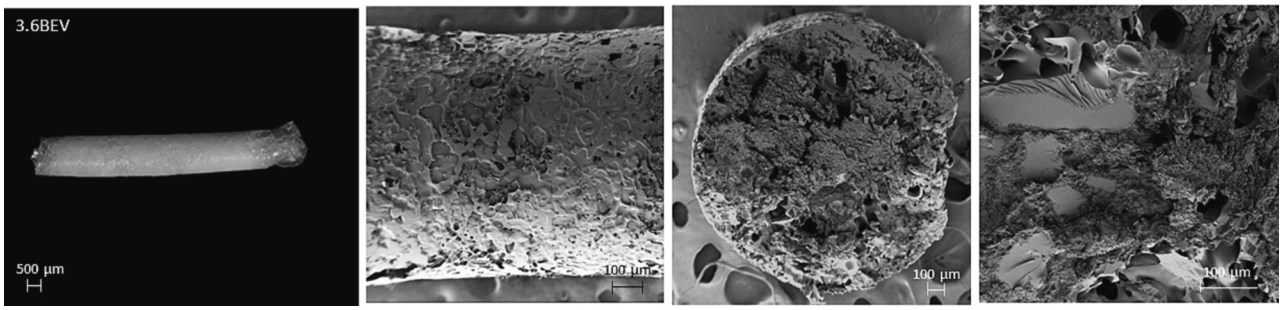

Fig. 10. Representative stereomicroscopy and SEM images of the surface and cross-sections of BEV implants produced by supercritical foaming.

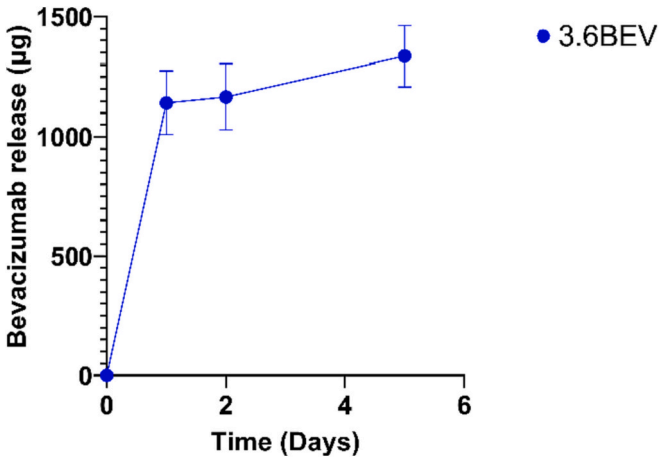

Fig. 11. *In vitro* release profile of BEV from 3.6BEV implants in PBS pH 7.4 (n = 3).

In contrast to the porous inner structure observed in DEX-loaded implants (Fig. 4), the drug-excipient patches present in the BEV-loaded implants functioned similarly to porogen agents, facilitating the accelerated release of the drug. When in contact with the pH 7.4 phosphate buffer medium, the BEV-HPβCD patches rapidly dissolved, resulting in almost complete drug release on the first day. The pH of the release medium was measured and found to decrease from its initial value of pH 7.4 to pH 6.75 by day 5.

Hydrophilic compounds, such as proteins or monoclonal antibodies, do not dissolve in CO_2, which is a non-polar molecule [60]. In contrast, DEX, which is non-polar in nature (logP = 1.83), quickly dissolves in CO_2 during the supercritical foaming process. The CO_2 then dissolves in the polymer, resulting in polymer swelling, which facilitates the embedding of the drug into the polymer matrix and ultimately the formation of the implant.

Supercritical foaming has previously been used successfully to incorporate hydrophilic drugs into polymeric matrices [61]. The hydrophilic/hydrophobic properties of the polymer matrix have a significant impact on hydrophilic drug loading. Polymer blends with a higher proportion of hydrophilic domains are more suitable for embedding hydrophilic compounds. RES and PUR PLGA polymers were initially selected for this study due to their acidic end groups, which make them more hydrophilic than PLGA polymers with ester end groups. However, this selection resulted in an extremely rapid release of the drug. To achieve the desired release profile, it would be necessary to select another PLGA combination, alter the polymer-BEV ratio, or eliminate additional excipients.

This work showcases the successful integration of biological drugs, such as BEV, into a PLGA matrix using supercritical foaming. It emphasises the importance of meticulous material selection and precise processing conditions when developing drug-loaded implants, as these variables greatly influence the release profile and effectiveness of the implant. Innovative techniques like three-dimensional (3D) printing have demonstrated promising capabilities in fabricating drug-loaded implants with tailored sizes and drug dosages [62,63]. However, many of these methods require elevated temperatures or organic solvents [13,15,64], which present the aforementioned drawbacks.

Supercritical foaming allowed the manufacturing of the implants without harsh conditions, which is ideal for processing thermolabile compounds. However, further optimisation of the implants dimensions and release profiles is required in view of clinical application. The creation of 3D printed moulds allowed the manufacturing of implants with the desired size. Implant dimensional modifications can be achieved simply by adjusting the size of the 3D printed moulds. The next steps would involve the use of PLGA polymers with different lactide/glycolide ratios to better fit BEV properties and better characterise BEV stability in the processed implant. This approach can also be applied to other monoclonal antibodies/proteins, as they may interact differently with the PLGA matrix, resulting in different release profiles. Through careful modulation of polymer composition and depressurisation rates, the implant can be customised to accommodate specific bioactive molecules.

Additionally, the capability of sterilising the implants directly after production, as demonstrated in a previous study [65], brings these implants closer to clinical implementation. In a prospective scenario, ophthalmologists could receive sterilised implants of the desired size and dosage, ready for administration. This approach offers a convenient and efficient solution for personalised treatment, with the potential to optimise the manufacturing process and facilitate widespread clinical adoption.

3.3. Biocompatibility assessment of the implants

3.3.1. Hen's egg test on the chorioallantoic membrane (HET-CAM)

Fig. 12 shows the results of the HET-CAM test. The images show that there was no haemorrhage, lysis, or coagulation after 300 s of contact between the release medium of the implants and the chorioallantoic membrane (Fig. 12E–L). The irritation score was null, indicating no difference between the negative control (Fig. 12A and B) and the formulations, in contrast to the positive control (Fig. 12C and D). The absence of significant changes in the membrane, as indicated by HET-CAM results, suggests that the implants have a reduced likelihood of causing eye irritation or damage. This observation implies a greater level of safety for ocular use.

3.3.2. Cytocompatibility studies with the ARPE-19 cell line

To assess the cytocompatibility of DEX-loaded implants, ARPE-19 cells were co-incubated with the release medium from the implants and a DEX solution containing the highest dose levels (1.08 mg/mL). A blank PLGA implant served as a control, and as shown in Fig. 13, the percentage changes in cell viability closely resembled those of untreated cells. PLGA is widely recognised as a biocompatible material and finds applications in various drug delivery systems and biomedical fields,

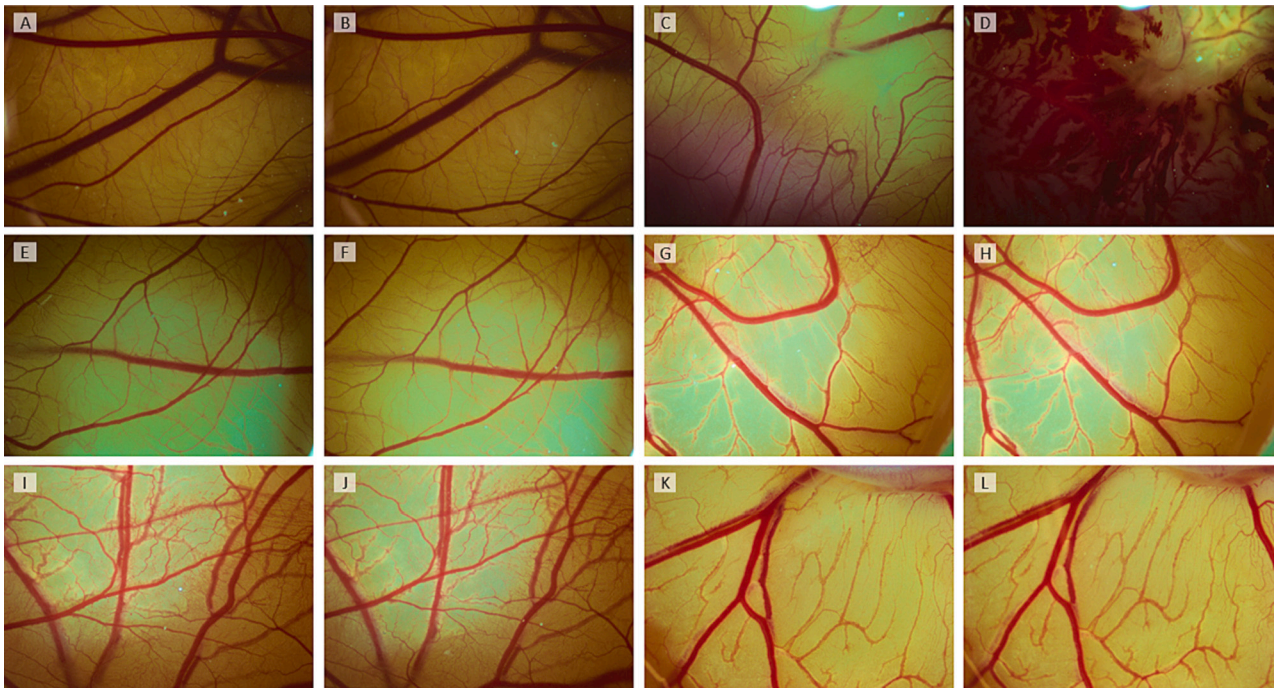

Fig. 12. Images of the chorioallantoic membrane before (A, C, E, G, I, K) and after 300 s of contact with negative control (B), positive control (D), 1.8DEX (F), 3.6DEX (H), 7.2DEX (J), and 3.6BEV (L) release medium.

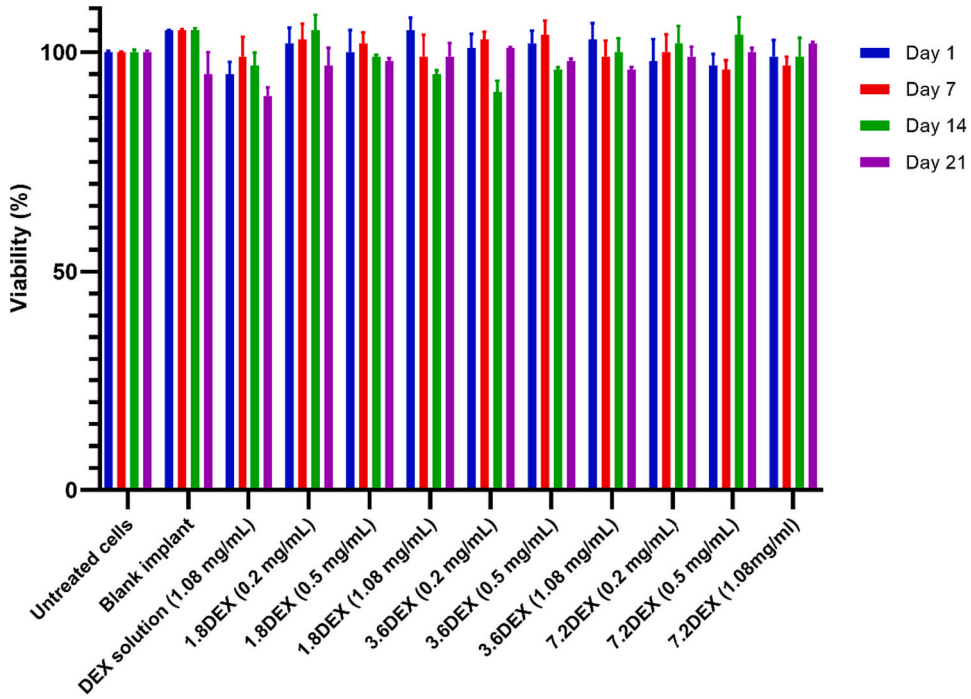

Fig. 13. Percentage changes in cell viability following co-incubation with cell culture medium (untreated cells), blank implants release medium, DEX solution, and DEX-loaded implants release medium for days 1, 7, 14 and 21.

including microspheres, tissue engineering scaffolds, and sutures [66,67].

The exposure of RPE cells to DEX-loaded implants containing different drug levels, as well as the DEX solution with the highest dose, did not have a significant impact on cell viability when compared to untreated cells. These findings indicate that DEX-loaded implants, within the clinically relevant intravitreal dosage range of 0.2–1.08 mg/mL, do not exhibit toxicity towards ARPE cells.

Nevertheless, there is still a concern regarding the influence of pH on the stability of DEX over an extended period of incubation. Despite the progressive degradation of PLGA over time, resulting in a decrease in pH as documented in this study and previous research [52,67], the pH of the cell culture medium remained consistently stable throughout the entire testing period (pH 7.2–7.4) owing to its effective buffering capacity. Multiple studies have demonstrated a decrease in cell viability for ARPE-19 cells when exposed to DEX for more than one day, despite an initial

boost in cell proliferation within the initial day of incubation [68]. Interestingly, DEX-loaded implants did not display any signs of toxicity, even at doses exceeding those used in clinical practice, within the first 24 h. However, it is worth noting that the observed lack of toxicity might be attributed to the degradation of the drug in the cellular medium at normal physiological pH, as previous research has indicated that DEX exhibits greater stability under acidic pH conditions [53]. Hence, these findings confirm the cytocompatibility of PLGA and suggest that clinical doses of DEX are seemingly well-tolerated by cells.

The cytocompatibility of BEV-loaded implants was also evaluated by comparing three different concentrations (0.047 mg/mL, 0.141 mg/mL, and 0.235 mg/mL) of BEV obtained from the release medium of the implants and from the commercial solution (Avastin®). To achieve equivalent concentrations of the implant release medium, the drug was diluted serially in a low serum culture medium. A blank PLGA implant served as a control, and as shown in Fig. 14, the cell viability percentage was comparable to that of untreated cells. High percentages of live cells were observed after co-incubation with the release medium on days 1 and 7, coinciding with complete drug release. The changes in cell viability percentage exhibited significant differences among all the groups for the three BEV concentrations ($p < 0.05$). Both BEV from the commercial solution and BEV released from the implants on day 1 stimulated more pronounced cell growth in ARPE-19 cells. However, the viability percentage for BEV released from the implants on day 7 approached values similar to the control group, albeit with a concentration-dependent impact on cell growth.

The observed effect appears to diminish over time, which may be attributed to the degradation of BEV in the cell culture medium or its potential adsorption to components within the medium [69]. In other investigations, ARPE-19 cells exposed to more concentrated BEV solutions exhibited similar viability values (close to 100%) as the control group [70,71]. These discrepancies could arise from variations in experimental conditions, cell culture protocols, or the specific assays employed to assess viability. While the precise mechanisms underlying the effects of BEV on ARPE-19 cells remain to be fully elucidated, it is important to note that no morphological changes were observed in these cells.

4. Conclusions

In this study, supercritical foaming technology was employed to prepare intravitreal PLGA implants loaded with dexamethasone. By manipulating the depressurisation rates during the foaming process, implants with desirable characteristics and customisable release patterns were successfully obtained. Notably, the dexamethasone implants exhibited improved release performance compared to previous studies [50,56–58], demonstrating their ability to release the drug in a controlled manner for up to 4 months. In view of these positive outcomes, the feasibility of incorporating bioactive molecules into the implants was explored, using the monoclonal antibody bevacizumab as a model drug. Through the same supercritical foaming process, a proof-of-concept investigation was conducted with bevacizumab-loaded implants. Further investigations will focus on optimising the implant dimensions and release patterns, with the ultimate goal of future clinical applications for the treatment of chronic retinal diseases. This study underscores the potential of supercritical foaming technology in the development of biocompatible intravitreal implants with precise release patterns and properties for the controlled delivery of drugs.

CRediT authorship contribution statement

Carlos Bendicho-Lavilla: Writing – review & editing, Writing – original draft, Methodology, Investigation, Formal analysis, Data curation, Conceptualization. **Iria Seoane-Viaño:** Writing – review & editing, Writing – original draft, Project administration, Methodology, Investigation, Formal analysis, Data curation, Conceptualization. **Víctor**

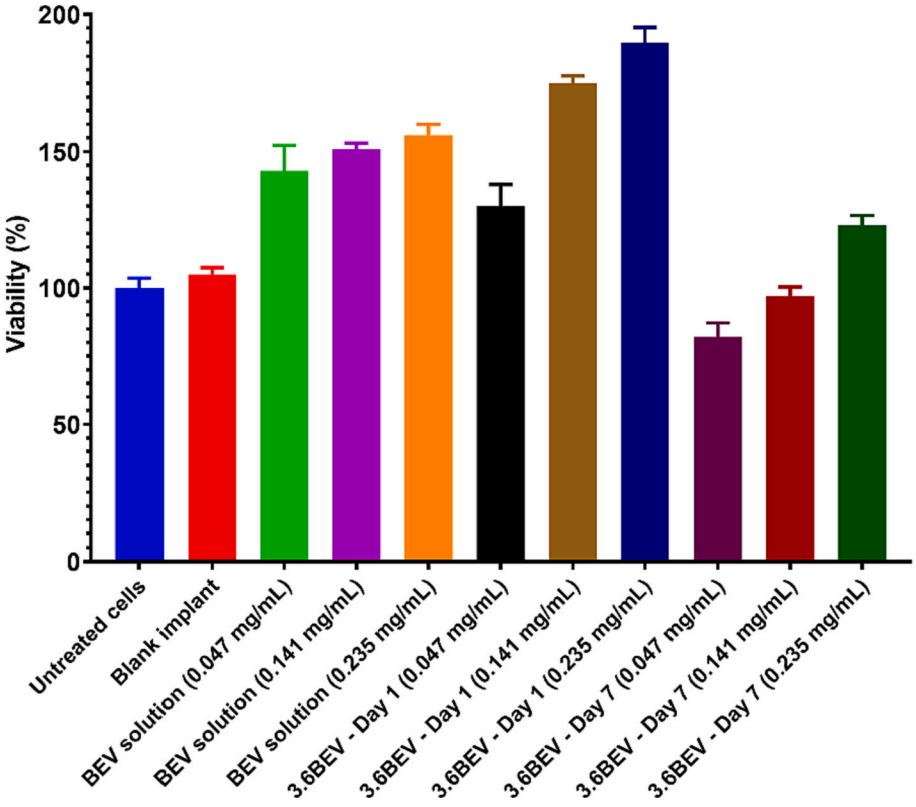

Fig. 14. Percentage changes in cell viability following co-incubation with varying concentrations of BEV from the implant release medium and the BEV commercial solution.

Santos-Rosales: Writing – review & editing, Writing – original draft, Methodology, Investigation, Formal analysis, Data curation, Conceptualization. **Victoria Díaz-Tomé:** Writing – review & editing, Methodology, Investigation. **María Carracedo-Pérez:** Methodology, Investigation. **Asteria M. Luzardo-Álvarez:** Writing – review & editing, Resources, Methodology, Investigation. **Carlos A. García-González:** Writing – review & editing, Resources, Funding acquisition. **Francisco J. Otero-Espinar:** Writing – review & editing, Supervision, Resources, Project administration, Methodology, Investigation, Funding acquisition, Formal analysis, Data curation, Conceptualization.

Data availability

Data will be made available on request.

Acknowledgements

I.S.-V. acknowledges Consellería de Cultura, Educación e Universidade for her Postdoctoral Fellowship (Xunta de Galicia, Spain; ED481B-2021-019). Work supported by MICINN [PID2022-142350OB-C21] and [PID2020-120010RB-I00], Xunta de Galicia [ED431C 2020/17], Agencia Estatal de Investigación [AEI] and FEDER funds. Authors would like to thank the use of RIAIDT-USC analytical facilities.

References

[1] Causes of blindness and vision impairment in 2020 and trends over 30 years, and prevalence of avoidable blindness in relation to VISION 2020: the right to sight: an analysis for the global burden of disease study, Lancet Glob. Health 9 (2021) e144–e160.
[2] R. Thapa, S. Khanal, H.S. Tan, S.S. Thapa, G. van Rens, Prevalence, Pattern and Risk Factors of Retinal Diseases among an Elderly Population in Nepal: The Bhaktapur Retina Study, Clinical Ophthalmology (Auckland, N.Z.) 14 (2020) 2109–2118.
[3] S.M. Kaiser, S. Arepalli, J.P. Ehlers, Current and future anti-VEGF agents for Neovascular age-related macular degeneration, J. Exp. Pharmacol. 13 (2021) 905–912.
[4] M.R. Munk, G.M. Somfai, M.D. de Smet, G. Donati, M.N. Menke, J.G. Garweg, L. Ceklic, The role of intravitreal corticosteroids in the treatment of DME: predictive OCT biomarkers, Int. J. Mol. Sci. 23 (2022) 7585.
[5] F. Ghanchi, R. Bourne, S.M. Downes, R. Gale, C. Rennie, I. Tapply, S. Sivaprasad, An update on long-acting therapies in chronic sight-threatening eye diseases of the posterior segment: AMD, DMO, RVO, uveitis and glaucoma, Eye 36 (2022) 1154–1167.
[6] M. Weber, M. Dominguez, F. Coscas, C. Faure, S. Baillif, L. Kodjikian, S.Y. Cohen, Impact of intravitreal aflibercept dosing regimens in treatment-naïve patients with neovascular age-related macular degeneration: 2-year results of RAINBOW, BMC Ophthalmol. 20 (2020) 206.
[7] S. Awwad, C. Henein, N. Ibeanu, P.T. Khaw, S. Brocchini, Preclinical challenges for developing long acting intravitreal medicines, Eur. J. Pharm. Biopharm. 153 (2020) 130–149.
[8] EMA, CHMP Assessment Report, 2010.
[9] S.S. Saincher, C. Gottlieb, Ozurdex (dexamethasone intravitreal implant) for the treatment of intermediate, posterior, and panuveitis: a systematic review of the current evidence, J. Ophthalmic Inflamm. Infect. 10 (2020) 1.
[10] M. Szymanska, D. Mahmood, T.E. Yap, M.F. Cordeiro, Recent advancements in the medical treatment of diabetic retinal disease, Int. J. Mol. Sci. 22 (2021) 9441.
[11] S.R. Chennamaneni, C. Mamalis, B. Archer, Z. Oakey, B.K. Ambati, Development of a novel bioerodible dexamethasone implant for uveitis and postoperative cataract inflammation, J. Control. Release 167 (2013) 53–59.
[12] J.Y. Won, J. Kim, G. Gao, J. Kim, J. Jang, Y.H. Park, D.W. Cho, 3D printing of drug-loaded multi-shell rods for local delivery of bevacizumab and dexamethasone: a synergetic therapy for retinal vascular diseases, Acta Biomater. 116 (2020) 174–185.
[13] I. Seoane-Viaño, P. Januskaite, C. Alvarez-Lorenzo, A.W. Basit, A. Goyanes, Semi-solid extrusion 3D printing in drug delivery and biomedicine: personalised solutions for healthcare challenges, J. Control. Release 332 (2021) 367–389.
[14] M. Almutairi, P. Srinivasan, P. Zhang, F. Austin, A. Butreddy, M. Alharbi, S. Bandari, E.A. Ashour, M.A. Repka, Hot-melt extrusion coupled with pressurized carbon dioxide for enhanced processability of pharmaceutical polymers and drug delivery applications - an integrated review, Int. J. Pharm. 629 (2022) 122291.
[15] F. Annuryanti, J. Domínguez-Robles, Q.K. Anjani, M.F. Adrianto, E. Larrañeta, R.R. S. Thakur, Fabrication and characterisation of 3D-printed triamcinolone acetonide-loaded polycaprolactone-based ocular implants, Pharmaceutics 15 (2023) 243.
[16] U. Angkawinitwong, S. Awwad, P.T. Khaw, S. Brocchini, G.R. Williams, Electrospun formulations of bevacizumab for sustained release in the eye, Acta Biomater. 64 (2017) 126–136.
[17] F. Chemat, M. Abert Vian, H.K. Ravi, B. Khadhraoui, S. Hilali, S. Perino, A.F. Tixier, Review of alternative solvents for green extraction of food and natural products: panorama, principles, applications and prospects, Molecules 24 (2019) 3007.
[18] S. Sharma, J. Das, W.M. Braje, A.K. Dash, S. Handa, A glimpse into green chemistry practices in the pharmaceutical industry, ChemSusChem 13 (2020) 2859–2875.
[19] P. Chakravarty, A. Famili, K. Nagapudi, M.A. Al-Sayah, Using supercritical fluid technology as a green alternative during the preparation of drug delivery systems, Pharmaceutics 11 (2019) 629.
[20] G. Gangapurwala, A. Vollrath, A. De San Luis, U.S. Schubert, PLA/PLGA-based drug delivery systems produced with supercritical CO(2)-a green future for particle formulation? Pharmaceutics 12 (2020) 1118.
[21] V. Santos-Rosales, I. Ardao, L. Goimil, J.L. Gomez-Amoza, C.A. García-González, Solvent-free processing of drug-loaded poly(ε-Caprolactone) scaffolds with tunable macroporosity by combination of supercritical foaming and thermal Porogen leaching, Polymers 13 (2021) 159.
[22] K.A. Kravanja, M. Finšgar, Ž. Knez, M. Knez Marevci, Supercritical fluid technologies for the incorporation of synthetic and natural active compounds into materials for drug formulation and delivery, Pharmaceutics 14 (2022) 1670.
[23] N.D. Machado, J.E. Mosquera, R.E. Martini, M.L. Goñi, N.A. Gañán, Supercritical CO2-assisted impregnation/deposition of polymeric materials with pharmaceutical, nutraceutical, and biomedical applications: a review (2015–2021), J. Supercrit. Fluids 191 (2022) 105763.
[24] E. Di Maio, E. Kiran, Foaming of polymers with supercritical fluids and perspectives on the current knowledge gaps and challenges, J. Supercrit. Fluids 134 (2018) 157–166.
[25] S. Milovanovic, D. Markovic, A. Mrakovic, R. Kuska, I. Zizovic, S. Frerich, J. Ivanovic, Supercritical CO(2) - assisted production of PLA and PLGA foams for controlled thymol release, Mater. Sci. Eng. C Mater. Biol. Appl. 99 (2019) 394–404.
[26] V. Santos-Rosales, M. Gallo, P. Jaeger, C. Alvarez-Lorenzo, J.L. Gómez-Amoza, C. A. García-González, New insights in the morphological characterization and modelling of poly(ε-caprolactone) bone scaffolds obtained by supercritical CO2 foaming, J. Supercrit. Fluids 166 (2020) 105012.
[27] J. Wang, Y. Zhang, J. Sun, Z. Jiao, Controllable fabrication of multi-modal porous PLGA scaffolds with different sizes of SPIONs using supercritical CO2 foaming, J. Appl. Polym. Sci. 139 (2022) 52287.
[28] M.B.C. de Matos, A.P. Piedade, C. Alvarez-Lorenzo, A. Concheiro, M.E.M. Braga, H. C. de Sousa, Dexamethasone-loaded poly(ε-caprolactone)/silica nanoparticles composites prepared by supercritical CO2 foaming/mixing and deposition, Int. J. Pharm. 456 (2013) 269–281.
[29] V. Santos-Rosales, I. Ardao, L. Goimil, J.L. Gomez-Amoza, C.A. García-González, Solvent-free processing of drug-loaded poly(ε-caprolactone) scaffolds with tunable macroporosity by combination of supercritical foaming and thermal porogen leaching, Polymers 13 (2021) 159.
[30] E. Khodaverdi, M. Reza Abbaspour, F. Oroojalian, N. Omidkhah, S. Hosseinnezahd, H. Kamali, F. Hadizadeh, Dexamethasone delivery of porous PEG-PCL-PEG scaffolds with supercritical carbon dioxide gas foaming, J. Drug Deliv. Sci. Technol. 66 (2021) 102547.
[31] X. Xu, A. Awad, P. Robles-Martinez, S. Gaisford, A. Goyanes, A.W. Basit, Vat photopolymerization 3D printing for advanced drug delivery and medical device applications, J. Control. Release 329 (2021) 743–757.
[32] S.H. Kim, Y. Jung, S.H. Kim, A biocompatible tissue scaffold produced by supercritical fluid processing for cartilage tissue engineering, Tissue Eng. Part C Methods 19 (2012) 181–188.
[33] C.-X. Chen, Q.-Q. Liu, X. Xin, Y.-X. Guan, S.-J. Yao, Pore formation of poly (ε-caprolactone) scaffolds with melting point reduction in supercritical CO2 foaming, J. Supercrit. Fluids 117 (2016) 279–288.
[34] F. Sousa, B. Sarmento, M.T. Neves-Petersen, Biophysical study of bevacizumab structure and bioactivity under thermal and pH-stresses, Eur. J. Pharm. Sci. 105 (2017) 127–136.
[35] T. Serno, J.F. Carpenter, T.W. Randolph, G. Winter, Inhibition of agitation-induced aggregation of an IgG-antibody by hydroxypropyl-beta-cyclodextrin, J. Pharm. Sci. 99 (2010) 1193–1206.
[36] J. Domján, P. Vass, E. Hirsch, E. Szabó, E. Pantea, S.K. Andersen, T. Vigh, G. Verreck, G. Marosi, Z.K. Nagy, Monoclonal antibody formulation manufactured by high-speed electrospinning, Int. J. Pharm. 591 (2020) 120042.
[37] T. Stolzke, F. Krieg, T. Peng, H. Zhang, O. Häusler, C. Brandenbusch, Hydroxylpropyl-beta-cyclodextrin as potential excipient to prevent stress-induced aggregation in liquid protein formulations, Molecules 27 (2022) 5094.
[38] E.M.A. (EMA), Cyclodextrins Used as Excipients, C.f.H.M.P. (CHMP) (Ed.), United Kingdom, 2017.
[39] L.H. Lucas, B.A. Ersoy, L.A. Kueltzo, S.B. Kueltzo, S.B Joshi, D.T. Brandau, N. Thyagarajapuram, L.J. Peek, C.R. Middaugh, Probing Protein Structure and Dynamics by Second-Derivative Ultraviolet Absorption Analysis of Cation-{pi}, Interactions, Protein Sci 15 (2023) 2228.
[40] ICCVAM, Recommended Test Method Protocol: Heng's Egg Test - Chorioallantoic Membrane (HET-CAM) Test Method, 2010.
[41] T.L. Riss, R.A. Moravec, A.L. Niles, S. Duellman, H.A. Benink, T.J. Worzella, L. Minor, Cell viability assays, in: S. Markossian (Ed.), et. al., *Assay Guidance Manual*, Eli Lilly & Company and the National Center for Advancing Translational Sciences, 2013.
[42] A. Al Rashid, W. Ahmed, M.Y. Khalid, M. Koç, Vat photopolymerization of polymers and polymer composites: processes and applications, Addit. Manuf. 47 (2021) 102279.
[43] S. Das, K.Y. Ng, Impact of glutaraldehyde on in vivo Colon-specific release of resveratrol from biodegradable pectin-based formulation, J. Pharm. Sci. 99 (2010) 4903–4916.

[44] Q. Zhu, J. Talton, G.F. Zhang, T. Cunningham, Z.J. Wang, R.C. Waters, J. Kirk, B. Eppler, D.M. Klinman, Y.J. Sui, S. Gagnon, I.M. Belyakov, R.J. Mumper, J. A. Berzofsky, Large intestine-targeted, nanoparticle-releasing oral vaccine to control genitorectal viral infection, Nat. Med. 18 (2012) 1291–1296.
[45] C. Zlomke, M. Barth, K. Mäder, Polymer degradation induced drug precipitation in PLGA implants - why less is sometimes more, Eur. J. Pharm. Biopharm. 139 (2019) 142–152.
[46] P.F.M. Oliveira, J.-F. Willart, J. Siepmann, F. Siepmann, M. Descamps, Using milling to explore physical states: the amorphous and polymorphic forms of dexamethasone, Cryst. Growth Des. 18 (2018) 1748–1757.
[47] L. Goimil, P. Jaeger, I. Ardao, J.L. Gómez-Amoza, A. Concheiro, C. Alvarez-Lorenzo, C.A. García-González, Preparation and stability of dexamethasone-loaded polymeric scaffolds for bone regeneration processed by compressed CO2 foaming, J. CO2 Util. 24 (2018) 89–98.
[48] R. Sanz-Horta, E. Martinez-Campos, C. García, H. Reinecke, A. Gallardo, J. Rodriguez-Hernandez, C. Elvira, Breath figures makes porous the “so-called” skin layer obtained in polymer foams prepared by supercritical CO2 treatments, J. Supercrit. Fluids 167 (2021) 105051.
[49] S.K. Goel, E.J. Beckman, Generation of microcellular polymeric foams using supercritical carbon dioxide. I: effect of pressure and temperature on nucleation, Polym. Eng. Sci. 34 (1994) 1137–1147.
[50] E. Lehner, D. Gündel, A. Liebau, S. Plontke, K. Mäder, Intracochlear PLGA based implants for dexamethasone release: challenges and solutions, Int. J. Pharm.: X 1 (2019) 100015.
[51] H. Keles, A. Naylor, F. Clegg, C. Sammon, Investigation of factors influencing the hydrolytic degradation of single PLGA microparticles, Polym. Degrad. Stab. 119 (2015) 228–241.
[52] C. Bassand, L. Benabed, J. Freitag, J. Verin, F. Siepmann, J. Siepmann, How bulk fluid renewal can affect in vitro drug release from PLGA implants: importance of the experimental set-up, Int. J. Pharm. X 4 (2022) 100131.
[53] I. González-García, A. Santoveña-Estévez, N. Teigell-Pérez, J.B. Fariña, D. Dorta-Vera, J. Suárez-González, Safe use of dexamethasone in pediatrics: design and evaluation of a novel stable oral suspension, Pharm. Technol. Hosp. Pharm. 3 (2018) 59–70.
[54] B. Matter, A. Ghaffari, D. Bourne, Y. Wang, S. Choi, U.B. Kompella, Dexamethasone degradation in aqueous medium and implications for correction of in vitro release from sustained release delivery systems, AAPS PharmSciTech 20 (2019) 320.
[55] B. Matter, A. Ghaffari, D. Bourne, Y. Wang, S. Choi, U.B. Kompella, Dexamethasone degradation during in vitro release from an intravitreal implant, Invest. Ophthalmol. Vis. Sci. 57 (2016) 4010.
[56] M.A. Costello, J. Liu, B. Chen, Y. Wang, B. Qin, X. Xu, Q. Li, N.A. Lynd, F. Zhang, Drug release mechanisms of high-drug-load, melt-extruded dexamethasone intravitreal implants, Eur. J. Pharm. Biopharm. 187 (2023) 46.
[57] R. Bhagat, J. Zhang, S. Farooq, X.-Y. Li, Comparison of the release profile and pharmacokinetics of intact and fragmented dexamethasone intravitreal implants in rabbit eyes, J. Ocul. Pharmacol. Ther. 30 (2014) 854–858.
[58] R.A. Kelley, A. Ghaffari, Y. Wang, S. Choi, J.R. Taylor, R.R. Hartman, U. B. Kompella, Manufacturing of dexamethasone–poly(d,l-lactide-co-glycolide) implants using hot-melt extrusion: within- and between-batch product performance comparisons, J. Ocul. Pharmacol. Ther. 36 (2020) 290–297.
[59] R. Ragone, G. Colonna, C. Balestrieri, L. Servillo, G. Irace, Determination of tyrosine exposure in proteins by second-derivative spectroscopy, Biochemistry 23 (1984) 1871–1875.
[60] C. Ye, H. Chi, A review of recent progress in drug and protein encapsulation: approaches, applications and challenges, Mater. Sci. Eng. C 83 (2018) 233–246.
[61] M. Champeau, J.M. Thomassin, T. Tassaing, C. Jérôme, Drug loading of polymer implants by supercritical CO2 assisted impregnation: a review, J. Control. Release 209 (2015) 248–259.
[62] I. Seoane-Viaño, S.J. Trenfield, A.W. Basit, A. Goyanes, Translating 3D printed pharmaceuticals: from hype to real-world clinical applications, Adv. Drug Deliv. Rev. 174 (2021) 553–575.
[63] G. Tan, N. Ioannou, E. Mathew, A.D. Tagalakis, D.A. Lamprou, C. Yu-Wai-Man, 3D printing in ophthalmology: from medical implants to personalised medicine, Int. J. Pharm. 625 (2022) 122094.
[64] C. Bendicho-Lavilla, I. Seoane-Viaño, F.J. Otero-Espinar, A. Luzardo-Álvarez, Fighting type 2 diabetes: formulation strategies for peptide-based therapeutics, Acta Pharm. Sin. B 12 (2022) 621–636.
[65] V. Santos-Rosales, B. Magariños, C. Alvarez-Lorenzo, C.A. García-González, Combined sterilization and fabrication of drug-loaded scaffolds using supercritical CO(2) technology, Int. J. Pharm. 612 (2022) 121362.
[66] R. Varela-Fernández, C. Bendicho-Lavilla, M. Martin-Pastor, R. Herrero Vanrell, M. I. Lema-Gesto, M. González-Barcia, F.J. Otero-Espinar, Design, Optimization, and In Vitro Characterization of Idebenone-Loaded PLGA Microspheres for LHON Treatment, Int. J. Pharm 616 (2022) 121504.
[67] C. Bassand, J. Verin, M. Lamatsch, F. Siepmann, J. Siepmann, How agarose gels surrounding PLGA implants limit swelling and slow down drug release, J. Control. Release 343 (2022) 255–266.
[68] C.K. Yeung, K.P. Chan, C.K. Chan, C.P. Pang, D.S. Lam, Cytotoxicity of triamcinolone on cultured human retinal pigment epithelial cells: comparison with dexamethasone and hydrocortisone, Jpn. J. Ophthalmol. 48 (2004) 236–242.
[69] H. Liu, C. Nowak, M. Shao, G. Ponniah, A. Neill, Impact of Cell Culture on Recombinant Monoclonal Antibody Product Heterogeneity, 2016, pp. 1103–1112.
[70] D. Malik, M. Tarek, J. Caceres del Carpio, C. Ramirez, D. Boyer, M.C. Kenney, B. D. Kuppermann, Safety profiles of anti-VEGF drugs: bevacizumab, ranibizumab, aflibercept and ziv-aflibercept on human retinal pigment epithelium cells in culture, Br. J. Ophthalmol. 98 (Suppl. 1) (2014) i11–i16.
[71] S. Luthra, R. Narayanan, L.E. Marques, M. Chwa, D.W. Kim, J. Dong, G.M. Seigel, A. Neekhra, A.L. Gramajo, D.J. Brown, M.C. Kenney, B.D. Kuppermann, Evaluation of in vitro effects of bevacizumab (Avastin) on retinal pigment epithelial, neurosensory retinal, and microvascular endothelial cells, Retina (Philadelphia, Pa.) 26 (2006) 512–518.